FRONT MATTER

Title

Heterogeneous Integration of Rigid, Soft and Liquid Materials for Self-healable, Recyclable, and Reconfigurable Wearable Electronics

Teaser

Advances in materials, chemistry and mechanics enable self-healing, recycling and reconfiguring of wearable electronics

Authors

Chuanqian Shi[1,2,†], Zhanan Zou[2,†], Zepeng Lei[3], Pengcheng Zhu[2,4], Wei Zhang[3,*] and Jianliang Xiao[2,*]

Affiliations

[1]*School of Aerospace Engineering and Applied Mechanics, Tongji University, Shanghai 200092, China*
[2]*Department of Mechanical Engineering, University of Colorado Boulder, Boulder, Colorado 80309, USA*
[3]*Department of Chemistry, University of Colorado Boulder, Boulder, Colorado 80309, USA*
[4]*School of Materials Science and Engineering, Beihang University, Beijing, 100191, China*
†*These authors contributed equally.*
**To whom correspondence should be addressed. Email: Jianliang.Xiao@colorado.edu; Wei.Zhang@colorado.edu*

Abstract

Wearable electronics can be integrated with human body for monitoring physical activities and health conditions, for human-computer interfaces, and for virtual/augmented reality. We here report a multifunctional wearable electronic system that combines advances in materials, chemistry and mechanics to enable superior stretchability, self-healability, recyclability and reconfigurability. This electronic system heterogeneously integrates rigid, soft and liquid materials through a low-cost fabrication method. The properties reported in this wearable electronic system can find applications in many areas, including health care, robotics, and prosthetics, and can benefit the wellbeing, economy, and sustainability of our society.

MAIN TEXT

Introduction

Stretchable/flexible electronics has attracted tremendous attention in the past 2-3 decades due to the combination of its superior mechanical attributes and electrical performance*(1–4)*. It can be applied in places that are not accessible by traditional rigid printed circuit boards (PCBs), such as seamless integration with soft tissues and organs of human body for healthcare*(5–7)*, bio-inspired curvilinear imagers*(8–11)* and artificial skins that mimic the mechanical and electrical properties of natural skin*(12–14)*. Among all the exciting applications, wearable electronics represents one of the most important, as it is the most accessible to people, and can be integrated onto the surface of human body to provide many useful functions, including physical activity tracking*(15, 16)*, health monitoring*(17, 18)*, drug delivery*(19)*, human-computer interface*(20, 21)*, and virtual/augmented reality*(22)*. To achieve excellent mechanical compliance and electrical performance simultaneously, integration techniques that combine stretchable substrates, interconnects, and hard commercial chip components were developed, including soft microfluidic assemblies*(15)*, solderable and stretchable platforms*(23–25)*, and liquid metal based systems*(26, 27)*. More recently, various chemistry and mechanisms have been explored to enable self-healability*(28–32)* and degradability*(7, 33)* in wearable electronics. For example, microvascular agents*(28)*, dynamic covalent bonds*(31)*, metal-ligand supramolecular chemistry*(34)*, and hydrogen bonds*(35, 36)* have been studied to realize self-healable electronics, for improved reliability, durability, and cost*(37, 38)*. Among these mechanisms, polymer networks with covalent bonding demonstrate advantages in robustness, stability and mechanical strength when compared with non-covalent chemistry*(39)*.

All these developments could lead to an exciting bright future of applying technological advancements to improve the wellbeing of people and the society. However, on the other hand, mass production and application of electronics generate a large amount of electronic waste. By 2021, the total electric waste is estimated to reach 52.2 million tons, and the majority of the waste cannot be appropriately recycled*(40)*. The consequence is that a large amount of heavy metals and other hazardous substances have been entering the eco-system, causing serious environmental problems and human health issues*(41, 42)*. To resolve this issue, dynamic covalent thermoset polyimine has been developed, which can be not only self-healable/rehealable but also recyclable*(43–47)*. Based on the polyimine chemistry and its nanocomposites, we have recently reported a rehealable, fully recyclable, and malleable electronic skin*(29)*. However, the electronic skin reported in this work has limited compliance and stretchability (failure strain ~4%, Young's modulus ~10 MPa). And the resistivity (~1×10^{-3} Ω·cm) of the nanocomposite is too high for high-performance electronics. Furthermore, the rehealing process requires heat press, which is not ideal for wearable devices. Thus this previously reported polyimine and its nanocomposites are not optimal for stretchable, compliant, and self-healable electronics.

Here, we report a multifunctional wearable electronic system that can simultaneously provide full recyclability, excellent mechanical stretchability, self-healability and reconfigurability based on modified polyimine chemistry. Such wearable electronics is achieved by heterogeneous integration of rigid (chip components), soft (dynamic covalent thermoset polyimine, new formula) and liquid (eutectic liquid metal) materials through advanced mechanical design and low-cost fabrication method. In such wearable electronic system, off-the-shelf chip components provide high-performance sensing and monitoring of the human body, including physical motion tracking, temperature monitoring, and sensing of acoustic and electrocardiogram (ECG) signals. They are interconnected by intrinsically stretchable and robust liquid metal circuitry, and encapsulated by dynamic covalent thermoset polyimine matrix. Bond exchange reactions in the polyimine network, together with the flowability of liquid metal, enable the wearable electronics to self-heal from damages and to be reconfigured into distinct configurations for different application scenarios. Furthermore, through transimination reactions, the polyimine matrix can be depolymerized into oligomers/monomers that are soluble in methanol and are separated from the chip components and liquid metal. All recycled materials and components can be reused to fabricate new materials and devices.

Results

The multifunctional wearable electronics incorporates three sensing modules: (i) electrocardiograph (ECG) sensor implemented by operational amplifiers and resistors, (ii) thermometer sensor for body temperature sensing, and (iii) accelerometer for acoustic and motion sensing (Fig. 1A). Figure 1B provides an exploded view of the schematic illustration of the design, which includes eutectic gallium-indium (EGaIn) liquid metal (LM) alloy, and commercial small-scale chip components encapsulated between two thin elastomeric polyimine membranes (Fig. S1A). The LM serves as electrical interconnects between chips, and each chip's pins are mounted precisely onto the patterned LM contact pads, similar to printed circuit boards but without the need of welding (Figs. S1B and S1C). The device in this case includes 12 chip components, the specifications of which are summarized in table S1. The LM circuitry in this multifunctional wearable electronics provides a combination of excellent electrical conductivity (3.4×10^6 S/m*(48)*) and superior intrinsic mechanical softness and deformability, so that the device can be crumpled when attached on human skin (Fig. 1C, top left), bended (Fig. 1C, top right), twisted (Fig. 1C, bottom left) and stretched (Fig. 1C, bottom right).

The stretchable substrate, insulation and encapsulation films in this wearable electronics are made of polyimine, which can be synthesized by using three commercially available monomers: terephthalaldehyde, 3,3′-diamino-*N*-methyldipropylamine and tris(2-aminoethyl)amine (Fig. S2A). As schematically illustrated in Fig. 1D, the cross-linked polyimine functions are based on the dynamic covalent chemistry principle*(39)*. A model reaction as shown in Fig. S2B clearly indicates the imine bond exchange reaction is efficient at both room temperature and 80 ºC. The FTIR spectra of terephthaldehyde and polyimine shown in Figure S2C further prove the full conversion of aldehyde into imine bonds. At appropriate environmental conditions, bond exchange reactions in polyimine network lead to effective stress relaxation, enabling excellent malleability and reprocessibility*(45–47)*. At the interface between two polyimine films, bond exchange reactions produce new covalent bonding across the interface, leading to effective interfacial bonding or healing. Another interesting characteristic of the polyimine network is that when excessive diamine and/or triamine monomers are introduced, transimination reactions lead to depolymerization of the polyimine network into oligomers/monomers soluble in methanol. This mechanism enables 100% recycling of the cross-linked polyimine. As shown in Fig. S2C, the high similarity between the FTIR spectra of the original and recycled polyimine supports the notion that these two films are chemically identical. Because of these properties of polyimine, the multifunctional wearable electronics is self-healable and fully recyclable (Fig. 1E). When the device is damaged, the broken pieces can be brought into contact, and bond exchange reactions can generate new covalent bonds at the interface. It should be noted, different from those self-healing materials using non-covalent supramolecular bonding interactions (e.g., hydrogen bonding, metal-ligand coordination, etc.), the polyimine matrix used herein consists of covalent bonds, thus making the devices much more robust and can operate under a broad range of conditions. The self-healed device regains both mechanical and electrical functions. When necessary, press can be used to improve interfacial contact and to accelerate bond exchange reactions for more effective interfacial healing. When the device is severely damaged or not needed, it can be fully recycled by soaking in the recycling solution, which is 3,3′-diamino-*N*-

methyldipropylamine and tris(2-aminoethyl)amine dissolved in methanol. When polyimine is completely depolymerized, the electrical components, including the chips and EGaIn LM, can be easily separated from the solution. The polymer solution and the electrical components can be reused for making new devices.

Fabrication of the multifunctional wearable electronics is schematically illustrated in Fig. 2A. It starts with mounting a silicon paper mask onto a synthesized polyimine film substrate. Screen printing method is adopted to brush EGaIn LM against the mask, and peeling off of the mask leaves patterned LM traces on the polyimine substrate. At each intersection of LM traces, a polyimine insulation layer is added. Then chip components are pick-and-placed onto the pre-designed locations with LM contact pads. Applying and curing uncured polyimine solution onto the device provides encapsulation and protection to the LM circuitry and chip components. This process is very low-cost, and compatible with printing technology.

The multifunctional wearable electronics integrates a thermal sensor (MCP9700, Microchip Technology), a triaxial accelerometer (ADXL335, Analog Devices Inc.), and a ECG sensor (AD8505, Analog Devices Inc. and Resistors, Bourns Inc.), so that it can provide real-time monitoring of body temperature, physical activities, health state, and also can serve as human-machine interfaces, as demonstrated in Figs. 2B-2E. The multifunctional wearable electronics can be worn on the wrist, to provide monitoring of physical activities, as shown in Fig. 2B. It can detect the different amplitude and frequency of walking, running and jumping. The thermal sensor can provide accurate measurement of body temperature in different environments and at different body locations. Figure 2C shows the measured forehead temperature when the subject stayed indoors (35.4 ºC) and outdoors (28.7 ºC) (top frame), and the different indoor temperatures on hand (33.6 ºC), lower abdomen (34.8 ºC) and forehead (35.4 ºC) (bottom frame). These measurements are consistent with the data obtained by using a commercial thermometer (Fig. S3A) *(49)*. When attached on the throat, the acoustic sensor can capture the vibration characteristics of the vocal cords, and serve as human-machine interfaces. As exhibited in Fig. 2D, the data captured clearly show distinct vibration signatures of different verbal commands, which are consistent with those obtained by using a commercial PC microphone (Fig. S3B). The ECG sensor monitors the electrocardiogram of the heart. The ECG data of the subject at rest, after exercised for 13 seconds and 34 seconds are presented in Fig. 2E. They correspond to the heart beating rate of 72/minute, 96/minute and 114/minutes, respectively. Refer to Supplementary Movie S1 for the real-time recording of the ECG data during exercising. To test biocompatibility, Figure S4 shows optical images comparing the skin conditions before (top left) and after wearing a polyimine film for 12 hours (bottom left) and 24 hours (bottom right), respectively. No noticeable adverse effects on the skin can be observed.

To ensure superior stretchability of the wearable electronics, both elastic polymer substrates and highly stretchable conductors are essential. The mechanical properties of the polyimine film are demonstrated in Fig. S5. The uniaxial stress-strain curve as shown in Fig. S5A exhibits a hyperelastic behavior of polyimine, and the initial slope gives the Young's modulus to be 2 MPa. Figure S5B shows the loading and unloading stress-strain curves of polyimine under cyclic loading test, which exhibits good elasticity with slight hysteresis. For the conductor, as LM is a liquid and can flow, it doesn't add rigidity to the wearable device and provides excellent deformability to the electronic system. How much the LM conductor can be stretched is limited by the polymer encapsulation. As shown in Fig. S6A the LM conductor encapsulated by polyimine can be stretched by ~200%.

Compared with stretchable conductors based on serpentine metal filamentary interconnects or buckled arc-shaped bridges*(12, 15)*, LM circuitry doesn't have fatigue issues, encapsulation doesn't affect the mechanical performance, and there is no stress concentration in the conductor at the interfaces between the rigid chip components and the soft substrate (Fig. S1C). Furthermore, the LM interconnects are robust and reliable under mechanical disturbances. As shown in Figs. S7A and S7B, the resistance of a polyimine encapsulated LM conductor subjected to repeated rubbing and pressing recovers to the original value when the mechanical forces are removed. These properties of the LM circuitry lead to superior mechanical stretchability, robustness and reliability in the multifunctional wearable electronics. Figure 3A shows an as-fabricated, undeformed multifunctional wearable device (left), and its finite element analysis (FEA) model (right). Figures 3B and 3C exhibit the multifunctional wearable device being uniaxially stretched by 60% along vertical and horizontal directions, respectively. The FEA results show that the maximum strains in the chip components are below 0.01%, far below the typical failure strain of silicon (~1%). Figure 3D presents the results of the device being stretched by 30% in both directions (areal strain ~70%). From FEA simulation, the maximum strain in the chip components is below 0.004%. The strain distributions in the polyimine substrate when the device is under different loading conditions are presented in Fig. S8. Figure S7C shows the resistance data of a LM conductor encapsulated by polyimine subjected to cyclic 60% strain. Since the resistance of the LM conductor is several orders of magnitude smaller than that of the electronic components shown in Table S1, the resistance change of the LM conductor during stretching should have negligible effect on the performance of the wearable device. Figure 3E exhibits the ECG data obtained by the wearable device under 30% biaxial stretching, and 60% uniaxial stretching along vertical and horizontal directions. The sensing performance of the other devices under different loading conditions is shown in Fig. S9. No noticeable influence of mechanical stretching on the sensing performance of the device is observed.

In addition to superior mechanical properties, the LM circuitry in polyimine matrix also provides excellent self-healing capability for the multifunctional wearable electronics. As demonstrated in Fig. 4A, when the LM circuit is cut broken by a razor blade (top frame), the ECG signal is lost (Fig. 4B, top). The top inset in Fig. 4A illustrates a magnified view of the broken LM conductor. After slightly pressing the two sides of the cut location, the LM conductor is self-healed, and the ECG sensor regains sensing capability (Fig. 4B, top, and Supplementary Movie S2). After the device self-heals for 13 minutes, the cut is optically invisible (Fig. 4A, middle), even under the optical microscope, as shown by the inset. After 48 hours of self-healing, bond exchange reactions at the interface lead to reformation of sufficient covalent bonds and effective interfacial healing. The mechanical strength of the healed interface is comparable to the original polyimine, as demonstrated by the tensile test results of self-healed LM conductors shown in Fig. S6A. Therefore, the self-healed multifunctional wearable electronics can be stretched by 60% (Fig. 4A, bottom, and Supplementary Movie S3), and the sensing performance is not affected (Fig. 4B, bottom). To effectively improve contact at the interface and to accelerate self-healing, some pressure can be applied on the broken device at room temperature. As shown in Figs. S6, C~G, by introducing a 90 g weight on the self-healing device, the self-healing time can be reduced to 144 minutes. When the weight is increased to 1000 g, the self-healing time can be further reduced to 13 minutes. All the self-healed devices show mechanical robustness and stretchability comparable to the original device (Fig. S6A). The sensing performances of the other devices, including motion, temperature, and acoustic sensing, are shown in Fig. S10A, which are also comparable to the original sensors. To further demonstrate the self-healing performance, the cutting and self-healing process at the same location of a polyimine encapsulated LM conductor was repeated for 5 times. As shown in Fig. S6B, the resistance recovers to the original value after 5 times cutting and self-healing. The stress-strain curve of the self-healed device shows elasticity comparable to the original device (Fig. S6A). As demonstrated in Fig. S6H, the LM conductor can still be stretched by 100% after 5 times self-healing.

Not only self-healable, the multifunctional electronics is also fully recyclable. When the multifunctional device is soaked in the recycling solution (Fig. 4C, top left), consisting of 3,3′-diamino-*N*-methyldipropylamine and tris(2-aminoethyl)amine in methanol, the excessive amine monomers can react with the imine bonds inside the polyimine network. Transimination reactions lead to depolymerization of polyimine into oligomers/monomers that are soluble in methanol. The top right and bottom right frames in Fig. 4C show the multifunctional device after being soaked in the recycling solution for 30 and 47 minutes. After 47 minutes, the polyimine matrix is completely depolymerized into oligomers/monomers and dissolved into methanol, the chip components and LM sink to the bottom of the container, which can be easily separated from the solution by using a paper filter. When an appropriate amount of terephthalaldehyde is added to rebalance the stoichiometry between the amine and aldehyde reactants, the recycled solution, chip components and LM can all be reused to make a new multifunctional device (Fig. 4C, bottom left). The recycling process was repeated for 3 times, and the electronic and mechanical performances of the recycled device are shown in Figs. 4D, 4F, and S10B. The new motion sensor fabricated using the recycled materials shows sensing performance comparable to the original device (Fig. 4D, and Supplementary Movie S4). The sensing performances of the other sensors in the recycled multifunctional device are shown in Fig. S10B. Figure 4E compares the mechanical property of the self-healed multifunctional electronics with the original device, along both horizontal and vertical directions, which show almost identical curves. The comparison between the recycled multifunctional electronics and the original device in Fig. 4F also shows almost identical mechanical properties in both directions.

The bond exchange reactions in the dynamic covalent polyimine network enable not only effective self-healing at the interfaces, but also stress relaxation in deformed material*(29, 45)*, which can be utilized to realize reconfigurable multifunctional electronics. This capability also partially attributes to the fluid behavior of the LM circuitry, as it doesn't add any rigidity or residual stress to the multifunctional wearable electronics. The time and temperature dependent relaxation behavior of the polyimine film can be characterized using dynamic mechanical analyzer (Model Q800, TA Instruments, New Castle, DE, USA). Figure S11A shows the dependence of storage modulus, loss modulus and tan δ over temperature, and it gives the glass transition temperature of polyimine as 21 °C. Figure S11B gives the results of a series of relaxation tests over a wide range of temperatures (12~80 °C). Specifically, at 60 °C, the relaxation modulus decreases from 1 MPa to 0.034 MPa in 10 minutes, which corresponds to 96.6% relaxation of the internal stress in the dynamic covalent network due to bond exchange reactions. By harnessing the effective stress relaxation in the polyimine network at elevated temperature and the fluid behavior of the LM circuitry, the multifunctional wearable electronics can be reconfigured into distinct configurations that suit for different application scenarios. As demonstrated in Fig. 5A, an initially flat multifunctional wearable device (160 mm long, the first configuration, top left) can be worn on the wrist by relaxing the stress induced by bending (bottom left). Then the device is stretched by 45% and heated to 60 °C to relax the stress, which yields the second flat configuration of the multifunctional device (232 mm long, top middle). It can be further wrapped onto the ankle and stress relaxation keeps the bent state of the device on the ankle (bottom middle). Further stretching the device by 112% and applying heat results in the third flat configuration of the multifunctional device (340 mm long, top right). It is then bent against the neck, and bending induced stress can also be relaxed to make sure the device stays on the neck for reliable sensing (bottom right). This process represents totally six different configurations. Optical microscope images in Fig. S1C prove robust connection between the LM circuitry and the rigid chip components under extreme deformation. Here, relatively thick polyimine films were used for the reconfigurable device, however, much thinner polyimine films can also be adopted, as shown in Fig. S5C, for improved flexibility and conformability. Figures 5B, 5C and 5D present the FEA simulation results of the flat states of the three different flat configurations. The maximum strains in the chip components are less than 0.01%, far below the failure strain of silicon (~1%). Figure 5E shows the ECG measurement from the device in its first configuration, worn on the wrist. Figure 5F presents the motion tracking data of the accelerometer in the multifunctional wearable electronics when it's worn on the ankle in the second configuration (Supplementary Movie S5). Figure 5G exhibits the acoustic sensing of the device in its third configuration, when wrapped around the neck (Supplementary Movie S6). The temperature monitoring at the wrist, the ankle and the neck in three different configurations of the same multifunctional wearable device is shown in Fig. 5H, indicating different temperature at different parts of the body, which agrees well with data obtained from a commercial thermometer. The sensing data of all the sensors in the wearable device in different configurations are presented in Fig. S12, proving robust sensing performance of the device during reconfiguration. Here, totally 5 times reconfiguration processes have been demonstrated. However, if the applied total stretch is kept below 200%, the device can be reconfigured for many times.

Discussion

We have demonstrated a highly stretchable, self-healable, recyclable and reconfigurable multifunctional wearable electronic system that can provide physical motion tracking, body temperature monitoring, and sensing of acoustic and ECG signals. The wearable electronics is realized by electrically interconnecting high-performance, off-the-shelf chip components using liquid metal circuity, and encapsulated with a dynamic covalent thermoset polyimine matrix. The wearable electronics can be stretched uniaxially by 60% in both horizontal and vertical directions and biaxially by 30% without affecting the electrical sensing performance. Enabled by the bond exchange reactions in the polyimine network and fluid behavior of the liquid metal circuitry, the wearable electronics can self-heal from damages, and can be reconfigured into distinct configurations for different application scenarios. When severely damaged or no longer needed, the wearable electronics can be fully recycled, leading to oligomers/monomers dissolved in methanol, and chip components and liquid metal can be separated from the solution. The recycled solution, chip components and liquid metal can be reused to make new-generation materials and devices. This work can find applications in many areas, including health care, prosthetics, robotics, and human-computer interfaces, and can benefit the wellbeing, economy, and sustainability our society.

Materials and Methods

Polyimine synthesis

To synthesize polyimine, terephthalaldehyde (1.5 g, 11.18 mmol), 3,3′-Diamino-*N*-methyldipropylamine (1.251 g, 8.61 mmol), and tris(2-aminoethyl)amine (0.252 g, 1.72 mmol) were mixed in methanol (20 mL), as shown in Fig. S2A. The solution was vigorously stirred and poured into a silicon paper mold, followed by evaporating methanol in a fume hood for 12 hours at room temperature and heat pressing at 80 °C and 8.5 kPa for 12 hours. For self-healable polyimine films, the solution was placed in fume hood for evaporating methanol for 2 hours at room temperature.

LM preparation

The LM used in this study is eutectic metal alloy consisting of gallium (75%) and indium (25%) (EGaIn, Sigma-Aldrich). Its melting temperature is 15.7 °C, and therefore maintains liquid state at room temperature. The resistivity of EGaIn is $29.4 \times 10^{-6}\ \Omega\cdot\text{cm}$*(48)*.

Fabrication of multifunctional wearable electronics

A silicon paper mask, made by laser cutting (Lide laser cutting machine) a 0.2 mm thick silicon paper film (Ruspepa non-stick silicone paper), was laminated over a polyimine film. Then LM was screen printed over the silicon paper mask using a razor blade. The liquid metal solidified after been cooled down to below 15.7 ºC. Removing the silicon paper mask left solidified LM traces on the polyimine film. After the temperature was raised to room temperature, the chip components were pick-and-placed on the pre-defined contact pads. The placement accuracy was ensured using an optical microscope. Pouring polyimine solution on top and curing at room temperature for 48 hours, the LM circuitry and chip components were encapsulated. For intersections, insulating polyimine was introduced to separate two crossing LM interconnects (Figs. 2A and S13A). The fabricated multifunctional electronics was then connected to external power source and data acquisition system using copper wires (Fig. S13B).

Self-healing and recycling process

To heal the broken polyimine device, an 1 kg weight was used to press polyimine for 13 minutes at room temperature to ensure good contact at the interface. Then the weight was removed, and the device was placed in a chemical hood for 48 hours.

The recycling solution was prepared by mixing 3,3′-Diamino-*N*-methyldipropylamine (0.417 g, 2.87 mmol) and tris(2-aminoethyl)amine (0.084 g, 0.574 mmol) in methanol. The device was then soaked in the recycling solution for 47 minutes to depolymerize the polyimine network into oligomers/monomers that can dissolve in methanol. After separating the LM and the chip components from the polymer solution, terephthalaldehyde (0.5 g, 3.72 mmol) was added into the polymer solution for synthesis of a new polyimine film. Diluted hydrochloric acid was used to remove the oxide layer on the surface of the LM, leading to congregation of LM*(50)*. Then both the LM and chip components can be cleaned using methanol.

Tension mechanical testing

Multifunctional wearable devices were tested using an Instron mechanical testing system, under quasi-static tension conditions*(51, 52)*. For multifunctional sensing devices, the samples were cut into rectangular ($40 \times 55\ \text{mm}^2$) shapes.

FEA simulation

To investigate the mechanical performance of the multifunctional wearable electronics, finite element analysis (FEA) was conducted using a commercial software package ABAQUS. The polyimine and LM were modeled as Neo-Hookean hyperelastic material using 3D hybrid stress elements (C3D8H), and the chip components were modeled using elastic isotropic material with 3D stress elements (C3D8). The Young's moduli and Poisson's ratios were 2 MPa and 0.35 for polyimine, and 160 GPa and 0.4 for the chip components*(53, 54)*. For simplicity, the LM circuitry was modeled as an extremely soft solid, with Young's modulus 10 Pa and Poisson's Ratio 0.5, which doesn't noticeably affect the mechanical behavior of the wearable electronic system, as the Young's modulus is 5 orders of magnitude smaller than polyimine.

Supplementary Materials

Chemical characterization of polyimine

Self-healing test and mechanical characterization.

Sensing performance test.

Isolation of wires at intersection.

Design of the circuit.

Fig. S1. (A) Multilayer construction of the multifunctional wearable electronics. (B) Optical images of the multifunctional wearable electronics from top view (top), tilted view (bottom left) and back view (bottom right). (C) Optical microscope images of the LM connection with the pins of chips at different configurations.

Fig. S2. (A) Polymerization of polyimine. (B) Model reaction design. Model reaction scheme includes the two reactants aa and bb, and the product ab (top). ^{1}H-NMR of aa, bb, mixture after 5 minutes at room temperature, mixture after 12 hours at room temperature, and mixture after 12 hours at 80ºC. A new peak corresponding to the N-CH_3 around 2.26 indicates the formation of ab (bottom). (C) FTIR of terephthalaldehyde (black), original polyimine (red) and recycled polyimine (blue).

Fig. S3. (A) Body temperature measurements from the wearable electronics compared with those from a commercial thermometer. (B) Acoustic data measured by the wearable electronics (top) and by a PC microphone (bottom).

Fig. S4. Optical images of skin before (top left) and after wearing a polyimine film (top right) for 12 hours (bottom left) and 24 hours (bottom right).

Fig. S5. (A) The uniaxial tension stress-strain curve of a polyimine film (left) and the linear fitting at small strain (right). (B) The loading and unloading stress-strain curves of the polyimine film. (C) Optical microscope image of the cross section of an 100 μm-thick polyimine film (left), and the optical image of this film being stretched by 100% (right).

Fig. S6. (A) Stress-strain curves of the original and self-healed films. (B) Resistance data of a polyimine encapsulated LM conductor during self-healing. Optical images of the LM conductor before (C) and after (D) cutting. The required self-healing time of polyimine encapsulated LM conductor with three different applied weights, 90 g (E), 400 g (F) and 1000 g (G). (H) The polyimine encapsulated LM conductor after 5 times self-healing. The self-healed films can be stretched by 100%.

Fig. S7. Resistance data of a polyimine encapsulated LM conductor subjected to rubbing (A) and pressing (B). (C) Resistance data of a polyimine encapsulated LM conductor subjected to cyclic 60% uniaxial strain.

Fig. S8. Max principal strain contours in polyimine when the multifunctional electronics is subjected to 30% biaxial strain (top), 60% uniaxial strain along vertical (middle) and horizontal (bottom) directions.

Fig. S9. (A) Motion data when the multifunctional electronics is subjected to 30% biaxial strain (top left), 60% uniaxial strain along horizontal (top right) and vertical (bottom left) directions. (B) Temperature data when the multifunctional electronics is subjected to 30% biaxial strain (top left) and 60% uniaxial strain along horizontal (top right) and vertical (bottom left) directions. The measurements using commercial thermometer are also shown for comparison.

Fig. S10. (A) Sensing performance of the self-healed device: Motion data (top left), Acoustic sensor data (top right), and Temperature measurements (compared with commercial thermometer results, bottom left). (B) Sensing performance of the recycled device: ECG signal (top left), Acoustic sensor data (top right), and Temperature data (compared with commercial thermometer results, bottom left).

Fig. S11. (A) Storage modulus, loss modulus and tan δ of polyimine versus temperature. (B) Relaxation test of polyimine at different temperatures.

Fig. S12. (A) ECG signals of the multifunctional wearable electronics in its second (left) and third (right) configurations. (B) Motion data of the multifunctional wearable electronics in its first (left) and third (right) configurations. (C) Acoustic sensor data of the multifunctional wearable electronics in its first (left) and second (right) configurations.

Fig. S13. (A) Optical image the LM circuitry (left), and optical microscope image of two crossing wires insulated using a polyimine interlayer (right). (B) Optical image of the cable for connecting the multifunctional wearable electronics with data acquisition equipment. (C) Circuit design of the multifunctional wearable electronics, the red lines mark the crossing wires.

Table S1. A list of the chip components used for the multifunctional wearable electronics.

Supplementary Movie S1. Real-time recording of the ECG data during exercising.

Supplementary Movie S2. ECG data during cutting and self-healing.

Supplementary Movie S3. Self-healed device subjected to stretching and bending.

Supplementary Movie S4. Motion data measured from a recycled device.

Supplementary Movie S5. Motion data of the device in its second configuration and wrapped around the ankle.

Supplementary Movie S6. Acoustic sensor data of the device in its third configuration and wrapped around the neck.

References and Notes

1. W. Gao, S. Emaminejad, H. Y. Y. Nyein, S. Challa, K. Chen, A. Peck, H. M. Fahad, H. Ota, H. Shiraki, D. Kiriya, D.-H. Lien, G. A. Brooks, R. W. Davis, A. Javey, Fully integrated wearable sensor arrays for multiplexed in situ perspiration analysis. *Nature* **529**, 509–514 (2016). doi:10.1038/nature16521

2. T. Sekitani, T. Yokota, U. Zschieschang, H. Klauk, S. Bauer, K. Takeuchi, M. Takamiya, T. Sakurai, T. Someya, Organic Nonvolatile Memory Transistors for Flexible Sensor Arrays. *Science* **326**, 1516–1519 (2009). doi:10.1126/science.1179963

3. J. A. Rogers, T. Someya, Y. Huang, Materials and mechanics for stretchable electronics. *Science* **327**, 1603–1607 (2010). doi: 10.1126/science.1182383

4. D.-H. Kim, J.-H. Ahn, W. M. Choi, H.-S. Kim, T.-H. Kim, J. Song, Y. Y. Huang, Z. Liu, C. Lu, J. A. Rogers, Stretchable and Foldable Silicon Integrated Circuits. *Science* **320**, 507–511 (2008). doi:10.1126/science.1154367

5. S. Choi, S. I. Han, D. Jung, H. J. Hwang, C. Lim, S. Bae, O. K. Park, C. M. Tschabrunn, M. Lee, S. Y. Bae, J. W. Yu, J. H. Ryu, S.-W. Lee, K. Park, P. M. Kang, W. B. Lee, R. Nezafat, T. Hyeon, D.-H. Kim, Highly conductive, stretchable and biocompatible Ag–Au core–sheath nanowire composite for wearable and implantable bioelectronics. *Nat. Nanotechnol.* **13**, 1048–1056 (2018). doi:10.1038/s41565-018-0226-8

6. I. R. Minev, P. Musienko, A. Hirsch, Q. Barraud, N. Wenger, E. M. Moraud, J. Gandar, M. Capogrosso, T. Milekovic, L. Asboth, R. F. Torres, N. Vachicouras, Q. Liu, N. Pavlova, S. Duis, A. Larmagnac, J. Vörös, S. Micera, Z. Suo, G. Courtine, S. P. Lacour, Electronic dura mater for long-term multimodal neural interfaces. *Science* **347**, 159–163 (2015). doi:10.1126/science.1260318

7. D. H. Kim, J. Viventi, J. J. Amsden, J. Xiao, L. Vigeland, Y. S. Kim, J. A. Blanco, B. Panilaitis, E. S. Frechette, D. Contreras, D. L. Kaplan, Dissolvable films of silk fibroin for ultrathin conformal bio-integrated electronics. *Nat. Mater* **9**, 511–517 (2010). doi:10.1038/nmat2745

8. Y. M. Song, Y. Xie, V. Malyarchuk, J. Xiao, I. Jung, K.-J. Choi, Z. Liu, H. Park, C. Lu, R. H. Kim, R. Li, K. B. Crozier, Y. Huang, J. A. Rogers, Digital cameras with designs inspired by the arthropod eye. *Nature* **497**, 95–99 (2013). doi:10.1038/nature12083

9. H. C. Ko, M. P. Stoykovich, J. Song, V. Malyarchuk, W. M. Choi, C.-J. Yu, J. B. Geddes III, J. Xiao, S. Wang, Y. Huang, J. A. Rogers, A hemispherical electronic eye camera based on compressible silicon optoelectronics. *Nature* **454**, 748–753 (2008). doi:10.1038/nature07113

10. C. Choi, M. K. Choi, S. Liu, M. S. Kim, O. K. Park, C. Im, J. Kim, X. Qin, G. J. Lee, K. W. Cho, M. Kim, E. Joh, J. Lee, D. Son, S. H. Kwon, N. L. Jeon, Y. M. Song, N. Lu, D. H. Kim, Human eye-inspired soft optoelectronic device using high-density MoS2-graphene curved image sensor array. *Nat. Commun.* **8**, 1664 (2017). doi:10.1038/s41467-017-01824-6

11. I. Jung, J. Xiao, V. Malyarchuk, C. Lu, M. Li, Z. Liu, J. Yoon, Y. Huang, J. A. Rogers, Dynamically tunable hemispherical electronic eye camera system with adjustable zoom capability. *Proc. Natl. Acad. Sci.* **108**, 1788–1793 (2011). doi:10.1073/pnas.1015440108

12. J. Kim, M. Lee, H. J. Shim, R. Ghaffari, H. R. Cho, D. Son, Y. H. Jung, M. Soh, C. Choi, S. Jung, K. Chu, D. Jeon, S.-T. Lee, J. H. Kim, S. H. Choi, T. Hyeon, D.-H. Kim, Stretchable silicon nanoribbon electronics for skin prosthesis. *Nat. Commun.* **5**, 5747 (2014). doi:10.1038/ncomms6747

13. D. J. Lipomi, V. Michael, B. C.-K. Tee, S. L. Hellstrom, J. A. Lee, C. H. Fox, Z. Bao, Skin-like pressure and strain sensors based on transparent elastic films of carbon nanotubes. *Nat. Nanotechnol.* **6**, 788–792 (2011). doi:10.1038/nnano.2011.184

14. G. Schwartz, B. C.-K. Tee, J. Mei, A. L. Appleton, D. H. Kim, H. Wang, Z. Bao, Flexible polymer transistors with high pressure sensitivity for application in electronic skin and health monitoring. *Nat. Commun.* **4**, 1859 (2013). doi:10.1038/ncomms2832

15. S. Xu, Y. Zhang, L. Jia, K. E. Mathewson, K.-I. Jang, J. Kim, H. Fu, X. Huang, P. Chava, R. Wang, S. Bhole, L. Wang, Y. J. Na, Y. Guan, M. Flavin, Z. Han, Y. Huang, J. A. Rogers, Soft microfluidic assemblies of sensors, circuits, and radios for the skin. *Science* **344**, 70–74 (2014). doi:10.1126/science.1250169

16. T. Yamada, Y. Hayamizu, Y. Yamamoto, Y. Yomogida, A. Izadi-najafabadi, D. N. Futaba, K. Hata, A stretchable carbon nanotube strain sensor for human-motion detection. *Nat. Nanotechnol.* **6**, 296–301 (2011). doi:10.1038/nnano.2011.36

17. R. C. Webb, A. P. Bonifas, A. Behnaz, Y. Zhang, K. J. Yu, H. Cheng, M. Shi, Z. Bian, Z. Liu, Y. Kim, W. Yeo, J. S. Park, J. Song, Y. Li, Y. Huang, A. M. Gorbach, J. A. Rogers, Ultrathin conformal devices for precise and continuous thermal characterization of human skin. *Nat. Mater.* **12**, 938–944 (2013). doi:10.1038/nmat3755

18. S. Y. Oh, S. Y. Hong, Y. R. Jeong, J. Yun, H. Park, S. W. Jin, G. Lee, J. H. Oh, H. Lee, S.-S. Lee, J. S. Ha, Skin-attachable, stretchable electrochemical sweat sensor for glucose and pH detection. *ACS Appl. Mater. Interfaces.* **10**, 13729–13740 (2018). doi:10.1021/acsami.8b03342

19. D. Son, J. Lee, S. Qiao, R. Ghaffari, J. Kim, J. E. Lee, C. Song, S. J. Kim, D. J. Lee, S. W. Jun, S. Yang, M. Park, J. Shin, K. Do, M. Lee, K. Kang, C. S. Hwang, N. Lu, T. Hyeon, D.-H. Kim, Multifunctional wearable devices for diagnosis and therapy of movement disorders. *Nat. Nanotechnol.* **9**, 397–404 (2014). doi:10.1038/nnano.2014.38

20. K. Sim, Z. Rao, Z. Zou, F. Ershad, J. Lei, A. Thukral, J. Chen, Q. Huang, J. Xiao, C. Yu, Metal oxide semiconductor nanomembrane–based soft unnoticeable multifunctional electronics for wearable human-machine interfaces. *Sci. Adv.* **5**, eaav9653 (2019). doi:10.1126/sciadv.aav9653

21. J. J. S. Norton, D. S. Lee, J. W. Lee, W. Lee, O. Kwon, P. Won, S.-Y. Jung, H. Cheng, J.-W. Jeong, A. Akce, S. Umunna, I. Na, Y. H. Kwon, X.-Q. Wang, Z. Liu, U. Paik, Y. Huang, T. Bretl, W. H. Yeo, J. A. Rogers, Soft, curved electrode systems capable of

integration on the auricle as a persistent brain-computer interface. *Proc. Natl. Acad. Sci.* **112**, 3920–3925 (2015). doi:10.1073/pnas.1424875112

22. X. Yu, Z. Xie, Y. Yu, J. Lee, A. Vazquez-Guardado, H. Luan, J. Ruban, X. Ning, A. Akhtar, D. Li, B. Ji, Y. Liu, R. Sun, J. Cao, Q. Huo, Y. Zhong, C. Lee, S. Kim, P. Gutruf, C. Zhang, Y. Xue, Q. Guo, A. Chempakasseril, P. Tian, W. Lu, J. Jeong9, Y. Yu, J. Cornman, C. Tan, B. Kim, K. Lee, X. Feng, Y. Huang, J. A. Rogers, Skin-Integrated Wireless Haptic Interfaces for Virtual and Augmented Reality. *Nature* **575**, 473–479 (2019). doi:10.1038/s41586-019-1687-0

23. Y. Kim, J. Lu, B. Shih, A. Gharibans, Z. Zou, K. Matsuno, R. Aguilera, Y. Han, A. Meek, J. Xiao, M. T. Tolley, T. P. Coleman, Scalable Manufacturing of Solderable and Stretchable Physiologic Sensing Systems. *Adv. Mater*. **29**, 1701312 (2017). doi: 10.1002/adma.201701312

24. Y. Liu, J. J. S. Norton, R. Qazi, Z. Zou, K. R. Ammann, H. Liu, L. Yan, P. L. Tran, K. Jang, J. W. Lee, D. Zhang, K. A. Kilian, S. H. Jung, T. Bretl, J. Xiao, M. J. Slepian, Y. Huang, J. Jeong, J. A. Rogers, Epidermal mechano-acoustic sensing electronics for cardiovascular diagnostics and human-machine interfaces. *Sci. Adv.* **2**, 1–12 (2016). doi: 10.1126/sciadv.1601185

25. S. Il Park, D. S. Brenner, G. Shin, C. D. Morgan, B. A. Copits, H. U. Chung, M. Y. Pullen, K. N. Noh, S. Davidson, S. J. Oh, J. Yoon, K. I. Jang, V. K. Samineni, M. Norman, J. G. Grajales-Reyes, S. K. Vogt, S. S. Sundaram, K. M. Wilson, J. S. Ha, R. Xu, T. Pan, T. Il Kim, Y. Huang, M. C. Montana, J. P. Golden, M. R. Bruchas, R. W. Gereau, J. A. Rogers, Soft, stretchable, fully implantable miniaturized optoelectronic systems for wireless optogenetics. *Nat. Biotechnol.* **33**, 1280–1286 (2015). doi: 10.1038/nbt.3415

26. Y. R. Jeong, J. Kim, Z. Xie, Y. Xue, S. M. Won, G. Lee, S. W. Jin, S. Y. Hong, X. Feng, Y. Huang, J. A. Rogers, J. S. Ha, A skin-attachable, stretchable integrated system based on liquid GaInSn for wireless human motion monitoring with multi-site sensing capabilities. *NPG Asia Mater.* **9**, e443 (2017). doi: 10.1038/am.2017.189

27. T. Lu, E. J. Markvicka, Y. Jin, C. Majidi, Soft-Matter Printed Circuit Board with UV Laser Micropatterning. *ACS Appl. Mater. Interfaces*. **9**, 22055–22062 (2017). doi: 10.1021/acsami.7b05522

28. K. S. Toohey, N. R. Sottos, J. A. Lewis, J. S. Moore, S. R. White, Self-healing materials with microvascular networks. *Nat. Mater.* **6**, 581–585 (2007). doi:10.1038/nmat1934

29. Z. Zou, C. Zhu, Y. Li, X. Lei, W. Zhang, J. Xiao, Rehealable, fully recyclable, and malleable electronic skin enabled by dynamic covalent thermoset nanocomposite. *Sci. Adv.* **4**, eaaq0508 (2018). doi:10.1126/sciadv.aaq0508

30. Y. Chen, A. M. Kushner, G. A. Williams, Z. Guan, Multiphase design of autonomic self-healing thermoplastic elastomers. *Nat. Chem.* **4**, 467–472 (2012). doi:10.1038/nchem.1314

31. B. B. J. Adzima, C. J. Kloxin, C. N. Bowman, Externally triggered healing of a thermoreversible covalent network via self-limited hysteresis heating. *Adv. Mater.* **22**, 2784–2787 (2010). doi:10.1002/adma.200904138

32. D. Son, J. Kang, O. Vardoulis, Y. Kim, N. Matsuhisa, J. Y. Oh, J. W. To, J. Mun, T. Katsumata, Y. Liu, A. F. McGuire, M. Krason, F. Molina-Lopez, J. Ham, U. Kraft, Y. Lee, Y. Yun, J. B.-H. Tok, Z. Bao, An integrated self-healable electronic skin system fabricated via dynamic reconstruction of a nanostructured conducting network. *Nat. Nanotechnol.* **13**, 1057 (2018). doi:10.1038/s41565-018-0244-6

33. S.-W. Hwang, H. Tao, D.-H. Kim, H. Cheng, J.-K. Song, E. Rill, M. A. Brenckle, B. Panilaitis, S. M. Won, Y.-S. Kim, Y. M. Song, K. J. Yu, A. Ameen, R. Li, Y. Su, M. Yang, D. L. Kaplan, M. R. Zakin, M. J. Slepian, Y. Huang, F. G. Omenetto, J. A. Rogers, A Physically Transient Form of Silicon Electronics. *Science* **337**, 1640–1644 (2012). doi:10.1126/science.1226325

34. Y. Shi, M. Wang, C. Ma, Y. Wang, X. Li, G. Yu, A Conductive Self-Healing Hybrid Gel Enabled by Metal-Ligand Supramolecule and Nanostructured Conductive Polymer. *Nano Lett.* **15**, 6276–6281 (2015). doi: 10.1021/acs.nanolett.5b03069

35. B. C. K. Tee, C. Wang, R. Allen, Z. Bao, An electrically and mechanically self-healing composite with pressure- and flexion-sensitive properties for electronic skin applications. *Nat. Nanotechnol.* **7**, 825–832 (2012). doi: 10.1038/nnano.2012.192

36. J. Y. Oh, S. Rondeau-Gagné, Y. C. Chiu, A. Chortos, F. Lissel, G. J. N. Wang, B. C. Schroeder, T. Kurosawa, J. Lopez, T. Katsumata, J. Xu, C. Zhu, X. Gu, W. G. Bae, Y. Kim, L. Jin, J. W. Chung, J. B. H. Tok, Z. Bao, Intrinsically stretchable and healable semiconducting polymer for organic transistors. *Nature*. **539**, 411–415 (2016). doi: 10.1038/nature20102

37. T. C. Mauldin, M. R. Kessler, Self-healing polymers and composites. *Int. Mater. Rev.* **55**, 317–346 (2010). doi: 10.1179/095066010X12646898728408

38. V. K. Thakur, M. R. Kessler, Self-healing polymer nanocomposite materials: A review. *Polymer.* **69**, 369–383 (2015). doi: 10.1016/j.polymer.2015.04.086

39. Y. Jin, C. Yu, R. J. Denman, W. Zhang, Recent advances in dynamic covalent chemistry. *Che. Soc. Rev.* **42**, 6634-6654 (2013). doi: 10.1039/C3CS60044K

40. S. M. Abdelbasir, S. S. M. Hassan, A. H. Kamel, R. S. El-Nasr, Status of electronic waste recycling techniques: a review. *Environ. Sci. Pollut. Res.* **25**, 16533–16547 (2018). doi:10.1007/s11356-018-2136-6

41. S.-R. Shin, V. D. Mai, D.-S. Lee, Chemical Recycling of Used Printed Circuit Board Scraps: Recovery and Utilization of Organic Products. *Processes* **7**, 22 (2019). doi:10.3390/pr7010022

42. A. K. Awasthi, X. Zeng, J. Li, Environmental pollution of electronic waste recycling in India: A critical review. *Environ. Pollut.* **211**, 259–270 (2016). doi:10.1016/j.envpol.2015.11.027

43. P. Taynton, C. Zhu, S. Loob, R. Shoemaker, J. Pritchard, Y. Jin, W. Zhang, Re-healable polyimine thermosets: polymer composition and moisture sensitivity. *Polym. Chem.* **7**, 7052–7056 (2016). doi: 10.1039/c6py01395c

44. J. M. Whiteley, P. Taynton, W. Zhang, S. H. Lee, Ultra-thin Solid-State Li-Ion Electrolyte Membrane Facilitated by a Self-Healing Polymer Matrix. *Adv. Mater.* **27**, 6922–6927 (2015). doi: 10.1002/adma.201502636

45. Y. Jin, , Z. Lei, P. Taynton, S. Huang, W. Zhang, Malleable and Recyclable Thermosets: The Next Generation of Plastics. Matter 1, 1456-1493 (2019). doi:10.1016/j.matt.2019.09.004

46. P. Taynton, K. Yu, R. K. Shoemaker, Y. Jin, H. J. Qi, W. Zhang, Heat- or Water-Driven Malleability in a Highly Recyclable Covalent Network Polymer. Adv. Mater. 26, 3938–3942 (2014). doi:10.1002/adma.201400317

47. P. Taynton, H. Ni, C. Zhu, K. Yu, S. Loob, Y. Jin, H. J. Qi, W. Zhang, Repairable woven carbon fiber composites with full recyclability enabled by malleable polyimine networks. Adv. Mater. 28, 2904-2909 (2016). doi:10.1002/adma.201505245

48. M. D. Dickey, R. C. Chiechi, R. J. Larsen, E. A. Weiss, D. A. Weitz, G. M. Whitesides, Eutectic Gallium-Indium (EGaIn): A Liquid Metal Alloy for the Formation of Stable Structures in Microchannels at Room Temperature. *Adv. Funct. Mater.* **18**, 1097–1104 (2008). doi:10.1002/adfm.200701216

49. F. Suarez, A. Nozariasbmarz, D. Vashaee, M. C. Öztürk, Designing thermoelectric generators for self-powered wearable electronics. *Energy Environ. Sci.* **9**, 2099–2113 (2016). doi:10.1039/c6ee00456c

50. D. Kim, P. Thissen, G. Viner, D.-W. Lee, W. Choi, Y. J. Chabal, J.-B. Lee, Recovery of nonwetting characteristics by surface modification of gallium-based liquid metal droplets using hydrochloric acid vapor. ACS Appl. Mater. Interfaces. 5, 179-185 (2013). doi:10.1038/am.2017.189

51. W. Grellmann, S. Seidler, "Mechanical Properties of Polymers" in *polymer testing* (Seidler, Hanser, Munich, 2007), pp.104–110.

52. "Standard Test Method for Tensile Properties of Plastics," ASTM D638 − 10 (2010). doi:10.1520/D0638-10

53. U. Bhaskar, V. Passi, S. Houri, E. Escobedo-Cousin, S. H. Olsen, T. Pardoen, J.-P. Raskin, On-chip tensile testing of nanoscale silicon free-standing beams. *J. Mater. Res.* **27**, 571–579 (2012). doi: 10.1557/jmr.2011.340

54. J. J. Wortman, R. A. Evans, Young's Modulus, Shear Modulus, and Poisson's Ratio in Silicon and Germanium. *J. Appl. Phys.* **36**, 153–156 (1965). doi:10.1063/1.1713863

Acknowledgments

Funding: Financial support from National Science Foundation (CMMI-1762324) is gratefully acknowledged. C.S. acknowledges financial support from China Scholarship Council (File No. 201706260019).

Author contributions: C.S., Z.Z., W.Z. and J.X. designed the experiments. C.S., Z.Z., Z.L., P.Z. performed the experiments and analysis. C.S., Z.Z., Z.L., W.Z. and J.X. wrote the paper.

Competing interests: Authors declare no competing interests.

Data and materials availability: All data are available in the main text or the supplementary materials.

Figures and Tables

Fig. 1. Design and schematic illustration of highly stretchable, self-healable and recyclable multifunctional wearable electronics. (A) Schematic illustration of a multifunctional wearable electronic system mounted on the hand, which integrates ECG, acoustic, motion and temperature sensing capabilities. **(B)** Exploded view of the multifunctional wearable electronics. **(C)** Optical images of the multifunctional device being crumpled on skin, bended, twisted and stretched. **(D)** Schematic illustration of the dynamic covalent thermoset polyimine: polymerization and depolymerization, and bond exchange reaction induced bond breaking and reforming. **(E)** Schematic illustration of self-healing and recycling of the multifunctional wearable electronics.

Fig. 2. Fabrication processes and sensing performance of the multifunctional wearable electronics. (A) Schematic illustration of the fabrication processes of the multifunctional wearable electronics. **(B)** Motion tracking performance with the multifunctional device worn on the wrist. **(C)** Indoor and outdoor body temperatures acquired using the wearable electronics mounted on the forehead (top), and comparison of measured indoor body temperatures when the wearable electronics is mounted at different locations (bottom). **(D)** Acoustic data acquired using the wearable electronics mounted on the neck. **(E)** ECG data acquired using the wearable electronics when the subject is at rest (top), and after exercising for 13 seconds (middle) and 34 seconds (bottom).

Fig. 3. Computational and experimental studies of the stretchability of the multifunctional wearable electronics. (A) Optical image of the undeformed device (left), and the FEA model for simulation (right). Optical images and max principal strain contours of the multifunctional wearable electronics being uniaxially stretched by 60% along vertical direction **(B)**, along horizontal direction **(C)**, and being biaxially stretched by 30% **(D)**. **(E)** ECG data of the same device under different deformation modes.

Fig. 4. Self-healing and recycling of the multifunctional wearable electronics. (A) Optical images of the multifunctional device during self-healing processes. The insets show optical microscope images of the cut at different self-healing stages. **(B)** The ECG data during cutting and self-healing (top), and the ECG data when the device is stretched by 60% after self-healing for 48 hours. **(C)** Optical images of the multifunctional device during recycling processes. **(D)** Motion tracking data measured using the recycled device. Comparison of the stress-strain curves between the original and self-healed multifunctional device **(E)**, and between the original and recycled multifunctional device **(F)**.

Fig. 5. Reconfiguration of the multifunctional wearable electronics. (A) The first (left), second (middle) and third (right) configurations of the multifunctional electronics in its flat states (top), and when its worn on the wrist, the ankle and the neck (bottom). The FEA model **(B)** and the max principal strain contours of the multifunctional device when it's stretched by 45% in the second configuration **(C)**, and when it's stretched by 112% in the third configuration **(D)**. **(E)** ECG data obtained using the multifunctional wearable device in its first configuration (on the wrist). **(F)** Motion tracking data obtained using the same device in its second configuration (on the ankle). **(G)** Acoustic data obtained using the same

device in its third configuration (on the neck). **(H)** Comparison of the body temperature measurements using the same wearable device in its first (on the wrist), second (on the ankle) and third (on the neck) configurations.

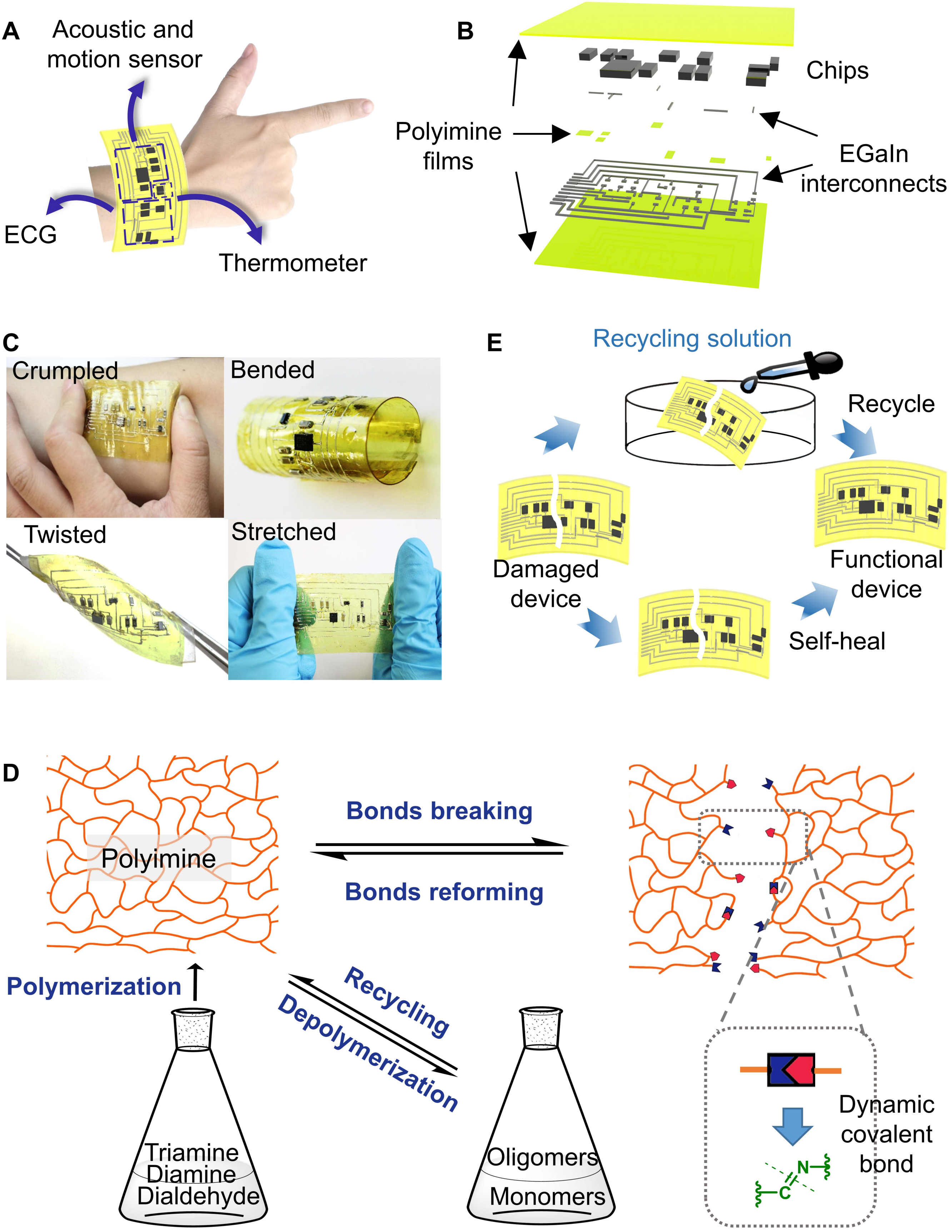
A
Acoustic and motion sensor
ECG
Thermometer
B
Chips
Polyimine films
EGaIn interconnects
C
Crumpled
Bended
Twisted
Stretched
E
Recycling solution
Recycle
Damaged device
Functional device
Self-heal
D
Polyimine
Bonds breaking
Bonds reforming
Polymerization
Recycling
Depolymerization
Triamine
Diamine
Dialdehyde
Oligomers
Monomers
Dynamic covalent bond
N
C

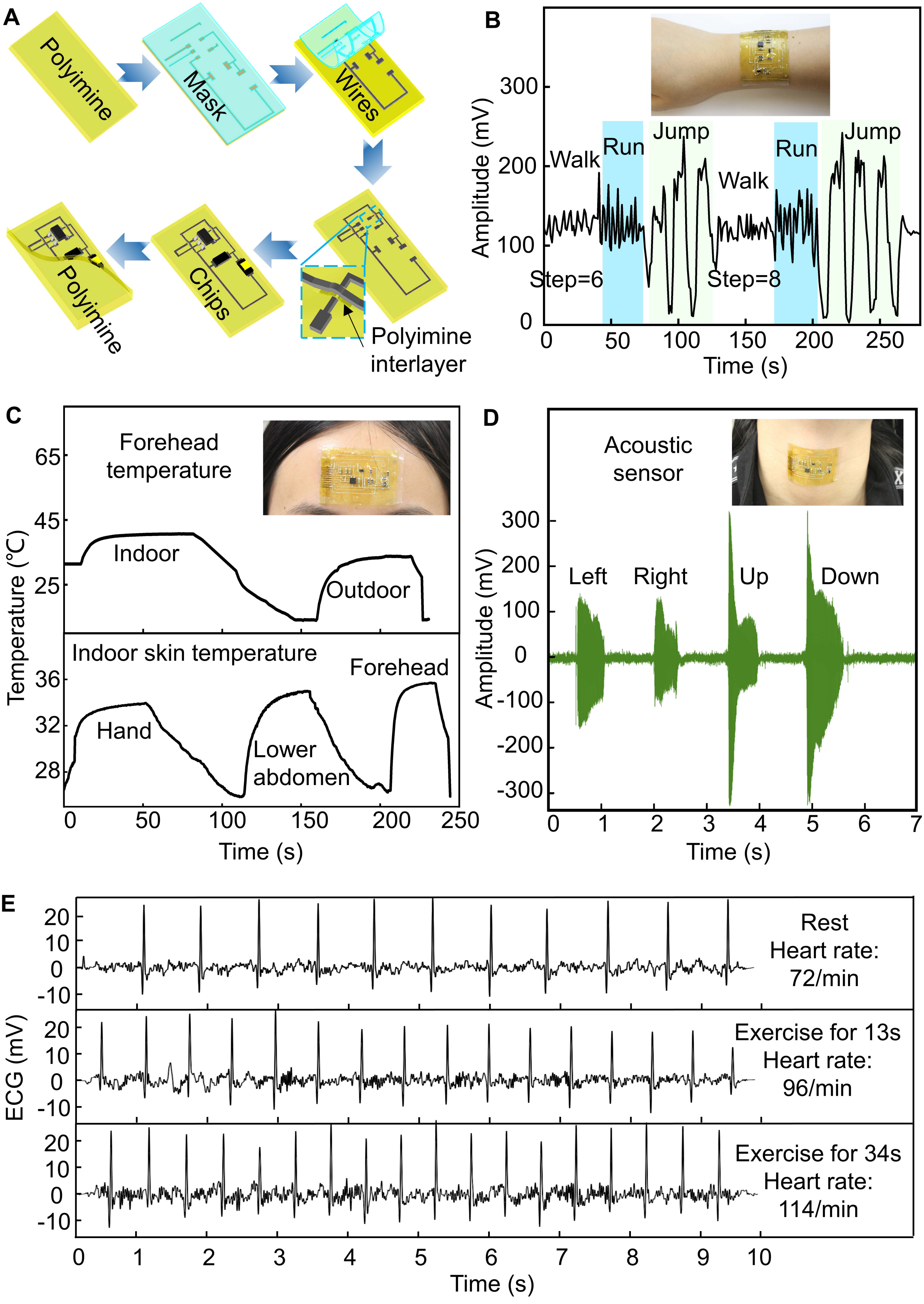
A
Polyimine
Mask
Wires
Polyimine interlayer
Chips
Polyimine
B
Amplitude (mV)
300
200
100
0
Walk
Run
Jump
Walk
Run
Jump
Step=6
Step=8
0
50
100
150
200
250
Time (s)
C
Forehead temperature
Indoor
Outdoor
65
45
25
Indoor skin temperature
Forehead
Hand
Lower abdomen
36
32
28
Temperature (°C)
0
50
100
150
200
250
Time (s)
D
Acoustic sensor
Amplitude (mV)
300
200
100
0
-100
-200
-300
Left
Right
Up
Down
0
1
2
3
4
5
6
7
Time (s)
E
ECG (mV)
20
10
0
-10
Rest
Heart rate: 72/min
Exercise for 13s
Heart rate: 96/min
Exercise for 34s
Heart rate: 114/min
0
1
2
3
4
5
6
7
8
9
10
Time (s)

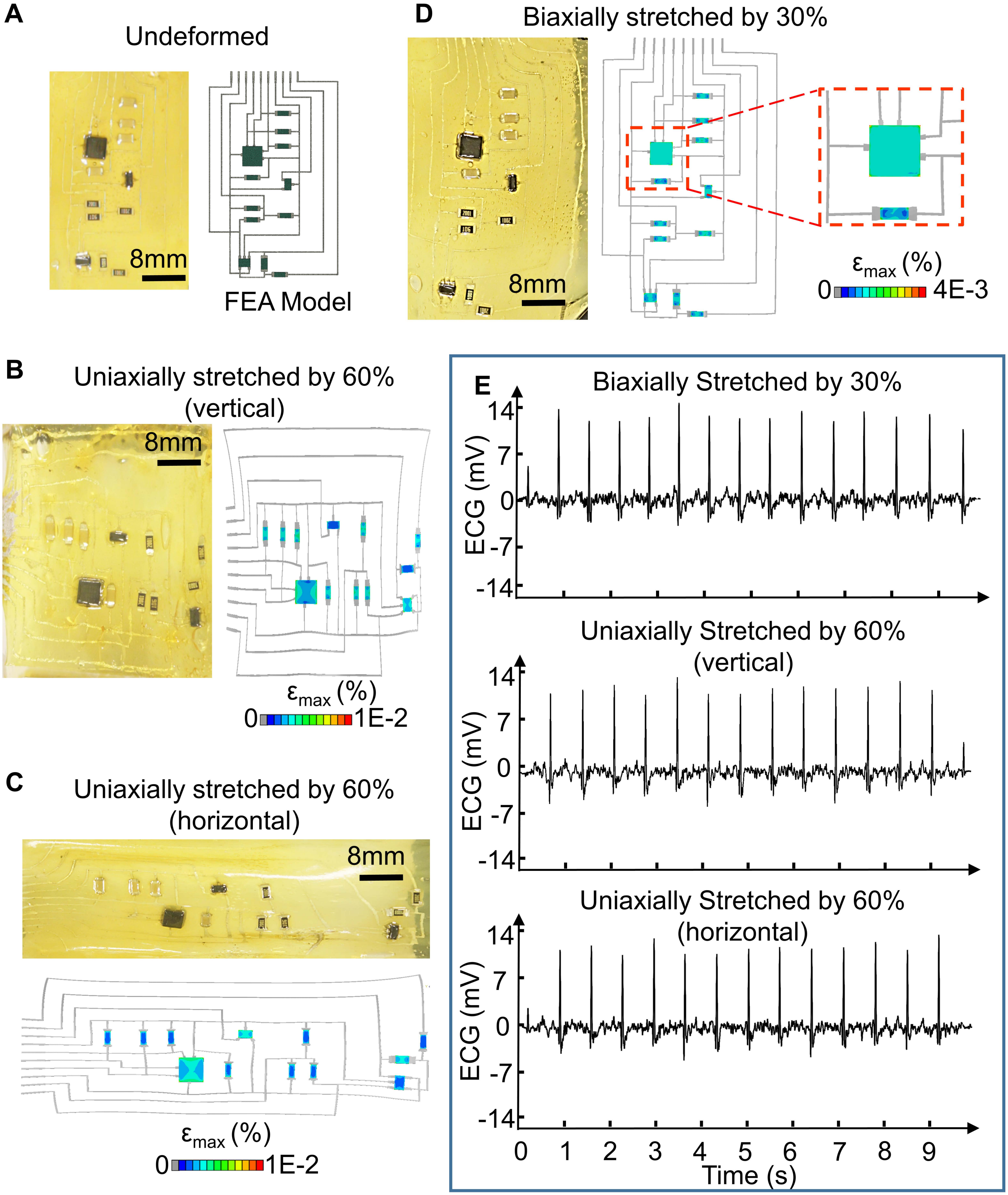
A
Undeformed
8mm
FEA Model
D
Biaxially stretched by 30%
8mm
εmax (%)
0
4E-3
B
Uniaxially stretched by 60%
(vertical)
8mm
εmax (%)
0
1E-2
C
Uniaxially stretched by 60%
(horizontal)
8mm
εmax (%)
0
1E-2
E
Biaxially Stretched by 30%
ECG (mV)
14
7
0
-7
-14
Uniaxially Stretched by 60%
(vertical)
ECG (mV)
14
7
0
-7
-14
Uniaxially Stretched by 60%
(horizontal)
ECG (mV)
14
7
0
-7
-14
0
1
2
3
4
5
6
7
8
9
Time (s)

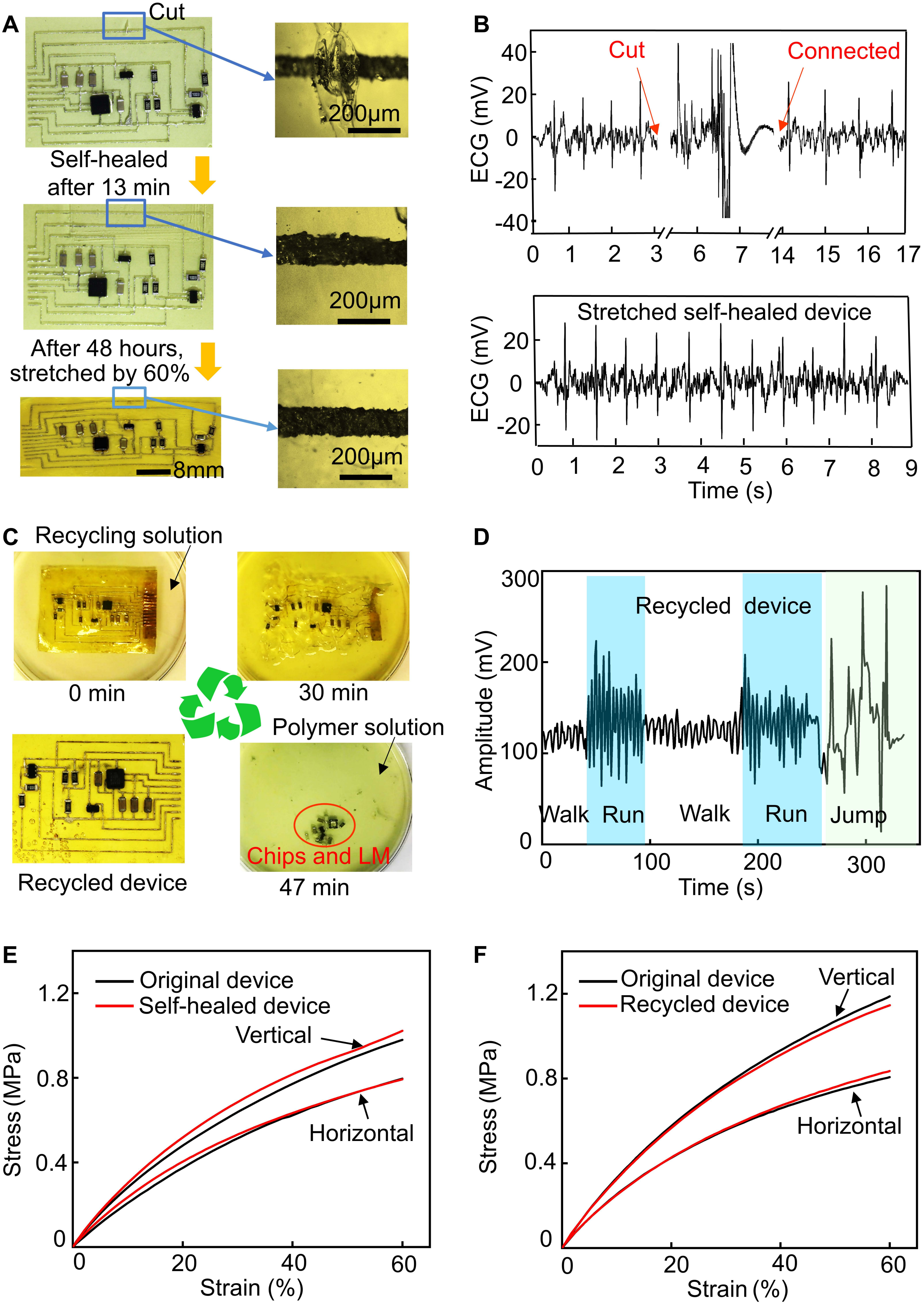
A
Cut
200µm
Self-healed after 13 min
200µm
After 48 hours, stretched by 60%
200µm
8mm
B
Cut
Connected
ECG (mV)
40
20
0
-20
-40
0 1 2 3 6 7 14 15 16 17
Stretched self-healed device
ECG (mV)
20
0
-20
0 1 2 3 4 5 6 7 8 9
Time (s)
C
Recycling solution
0 min
30 min
Polymer solution
Chips and LM
47 min
Recycled device
D
Recycled device
Amplitude (mV)
300
200
100
0
Walk
Run
Walk
Run
Jump
0 100 200 300
Time (s)
E
Original device
Self-healed device
Vertical
Horizontal
Stress (MPa)
1.2
0.8
0.4
0
0 20 40 60
Strain (%)
F
Original device
Recycled device
Vertical
Horizontal
Stress (MPa)
1.2
0.8
0.4
0
0 20 40 60
Strain (%)

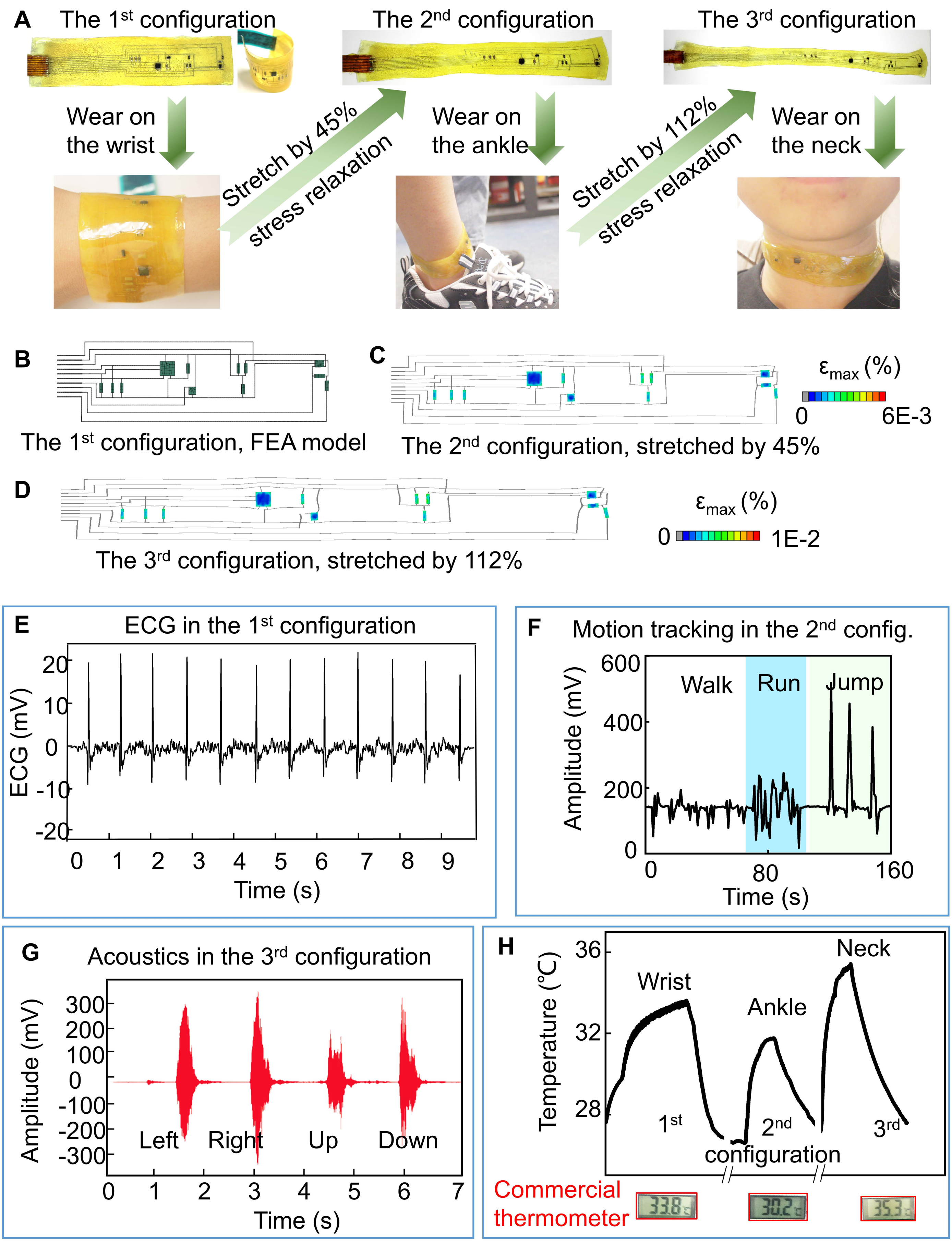
A
The 1st configuration
The 2nd configuration
The 3rd configuration
Wear on the wrist
Stretch by 45% stress relaxation
Wear on the ankle
Stretch by 112% stress relaxation
Wear on the neck
B
The 1st configuration, FEA model
C
The 2nd configuration, stretched by 45%
εmax (%)
0
6E-3
D
The 3rd configuration, stretched by 112%
εmax (%)
0
1E-2
E
ECG in the 1st configuration
ECG (mV)
20
10
0
-10
-20
0 1 2 3 4 5 6 7 8 9
Time (s)
F
Motion tracking in the 2nd config.
Amplitude (mV)
600
400
200
0
Walk
Run
Jump
0
80
160
Time (s)
G
Acoustics in the 3rd configuration
Amplitude (mV)
300
200
100
0
-100
-200
-300
Left
Right
Up
Down
0 1 2 3 4 5 6 7
Time (s)
H
Temperature (°C)
36
32
28
Wrist
Ankle
Neck
1st
2nd
3rd
configuration
Commercial thermometer
33.8
30.2
35.3